An *ab initio* molecular dynamics investigation of Li$_n$Al$_n$ clusters

Vaishali Shah†, D G Kanhere†‖, Chiranjib Majumder‡ and G P Das§¶

† Department of Physics, University of Poona, Pune 411 007, India
‡ Chemistry Division, Bhabha Atomic Research Centre, Bombay 400 085, India
§ Solid State Physics Division, Bhabha Atomic Research Centre, Bombay 400 085, India

Abstract. A systematic investigation of the ground-state geometries and stabilities of Li$_n$Al$_n$ ($n = 1$–10 and 13) clusters made by employing *ab initio* density-based molecular dynamics is reported. Although in the solid-state form, the 50:50 alloy takes on a B32-ordered structure, no evidence for such ordering has been seen for small clusters. Instead there is a clustering tendency of the Al atoms, and they tend to form inner clusters whose geometries are different from those of the free Al clusters. The Li and Al atoms favour a tetrahedral coordination due to the significant role of the s–p bonding of the electrons. A stability analysis based on energetics shows that the stability is enhanced in clusters where all of the Al faces have been capped by Li atoms, and this gives some remarkably interesting geometries, like the face-centred-cubic structure of Li$_8$Al$_6$.

1. Introduction

The advent of the density functional molecular dynamics method has given considerable impetus to *ab initio* investigation of small clusters. Such investigations are important, firstly because of the intrinsic physics of small and finite systems, and secondly because clusters serve as a prototype for obtaining an understanding of the properties of emerging novel materials such as nanoscale materials and cluster-assembled materials [1]. A significant number of the *ab initio* studies have been performed on homonuclear metallic and semiconducting clusters, with a view to obtaining an understanding of the equilibrium ground-state geometries, binding energies, relative stabilities (or abundances), reaction barriers, growth patterns, etc. These investigations, both experimental and theoretical, have revealed interesting features such as the existence of magic numbers, and have shown that the electronic and cohesive properties of clusters are quite different from those of the extended solids. However, much less work has been reported on heteronuclear clusters involving two or more species of atoms. In the present work, we focus our attention on heteronuclear clusters involving simple metal atoms, namely Li and Al, which serve as a model system, as we shall see later.

It is well known that in the solid phase, the Li and Al systems are miscible over the entire concentration range, and for the 50:50 concentration they form a stable ordered B32 intermetallic phase, whose bulk density of states (DOS) resembles that of a typical

‖ Electronic address: vaishali, kanhere@unipune.ernet.in.
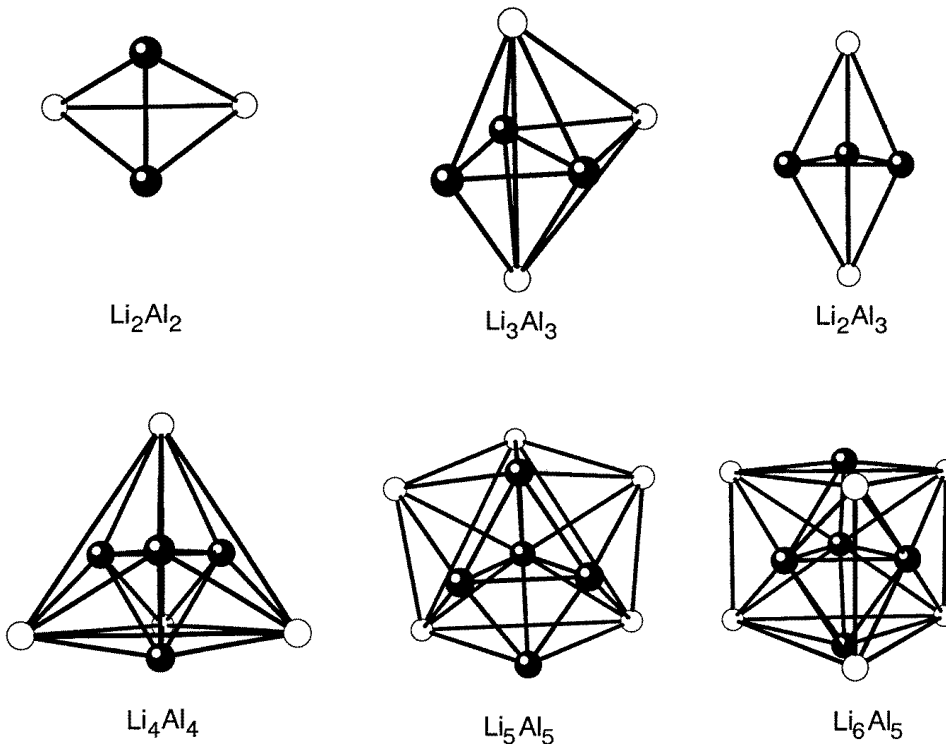¶ Electronic address: gpd@magnum.barc.ernet.in.

Figure 1. The ground-state geometries of the Li_nAl_n ($n = 2$–5), Li_2Al_3, and Li_6Al_5 clusters. The lighter spheres represent Li atoms and the darker spheres represent Al atoms.

covalently bonded diamond structure (without any band gap, of course) [2]. Each A atom (Li or Al) is surrounded by a fixed number of like (A) atoms and unlike (B) atoms as its first- and second-nearest neighbours, and in terms of the interaction potentials V_{jk} one can calculate the effective pair interaction (EPI) $J_2^{(i)} = V_{AA}^{(i)} + V_{BB}^{(i)} - 2V_{AB}^{(i)}$. Ordered superstructures appear only when $J_2^{(i)} > 0$. Let us recall that the process of collection of type A atoms in a localized region for attaining local enrichment is known as *clustering*, while the organization of type A and type B atoms in a superlattice structure gives rise to *ordering* in a binary AB alloy. These clustering and ordering tendencies cannot coexist if one considers only the first-nearest-neighbour interactions. The conditions under which clustering and ordering tendencies occur simultaneously or sequentially in an alloy have been investigated theoretically (from first principles) [3] in terms of the instabilities associated with the concentration fluctuations appropriate to the respective processes. For example in Al_3Li alloy, the metastable δ'-phase precipitates out as a result of the interplay between clustering and ordering processes.

It is instructive to see what happens to the clustering versus ordering behaviour in an AB alloy when one goes from solids to small clusters. In view of the fact that clusters are 'finite' systems having a 'surface', there are some inherent differences from a solid alloy which has an underlying infinite lattice with substitutional (i.e. chemical) disorder. So one cannot define here the ordering behaviour in terms of the EPIs, unlike in the case of solids. However, using *ab initio* molecular dynamics, it is possible to examine the evolution of the
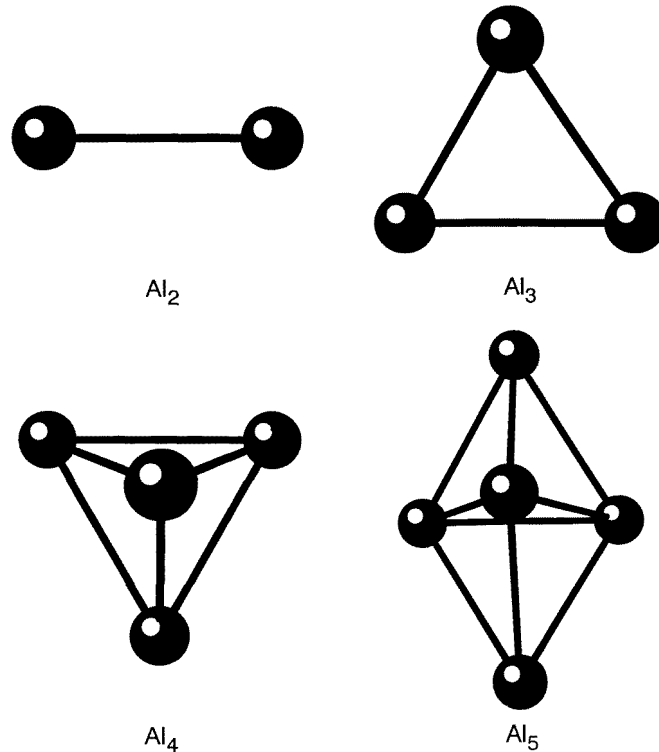
Figure 2. The geometries of the clusters of Al atoms within the ground-state configurations of Li$_n$Al$_n$ ($n = 2$–5) clusters.

stable ground-state geometry of an A$_n$B$_n$ cluster with increasing cluster size. In the early work on Al impurity in Li clusters [4, 5] evidence was found for localized bonding between Li and Al. Let us note that amongst the three bonds Al–Al, Li–Li, and Li–Al, the strongest is Li–Al and the weakest is Li–Li as seen in the diatomic system. Our preliminary study of Li$_7$Al$_n$ ($n = 1$–7) clusters [6] has revealed the following features.

(i) The ground-state geometries and stabilities of clusters appear to be dominated by the tetrahedral coordination between Li and Al atoms.

(ii) The Al atoms prefer to cluster together, and the geometries of these Al clusters differ significantly from those of free Al clusters with the same numbers of Al atoms.

Therefore, it is of considerable interest to carry out a detailed investigation on Li–Al clusters with equal concentrations of Li and Al. Our emphasis will be on looking for systematics in terms of clustering and ordering, evolutionary patterns as the contents of Li or Al are increased, systematics in terms of energetics and bond lengths, and the stabilities and geometries of such clusters, and on comparing these properties with the corresponding solid-state properties wherever possible. Towards this end, we have investigated the geometries, energetics, bond lengths, etc, for clusters of Li$_n$Al$_n$ ($n = 1$–10), Li$_{13}$Al$_{13}$, Li$_2$Al$_3$, Li$_6$Al$_5$, and Li$_8$Al$_6$. It turned out that the last three clusters emerged quite naturally out of our investigation as being very stable ones, and hence they were studied. Specifically, these clusters are characterized by the complete capping by Li atoms on all of the faces of the inner Al clusters.
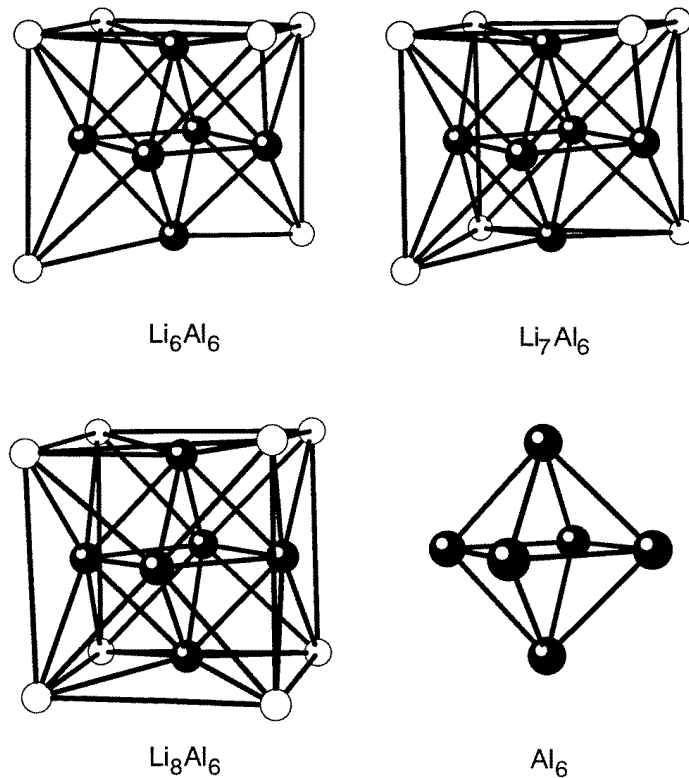
Figure 3. The ground-state geometries of the Li_6Al_6, Li_7Al_6, and Li_8Al_6 clusters. The lighter spheres again represent Li atoms and the darker spheres represent Al atoms. The inner octahedron of Al atoms is shown in the bottom right-hand corner of the figure.

We have chosen to use density-based molecular dynamics (DBMD) which has been shown to give correct ground-state geometries of small clusters containing simple metal atoms [7] except for the Jahn–Teller distortions. It is known to be stable over long simulated annealing runs, which are essential for treating heteroatomic clusters. The method has been very successfully used for calculating properties like ground-state configurations of c-Si and H/Si(100) 1×1, the free energy of formation of sodium vacancies and point defects, and the dynamical properties of liquids [8].

In the following section, a short description of the DBMD method is presented along with relevant numerical details of the calculations. This is then followed by the results and a discussion.

2. The method and numerical details

In the density-based molecular dynamics, the total energy of a system consisting of N_a atoms and N_e interacting electrons, under the influence of an external field due to the nuclear charges at coordinates R_n, can be written as a functional of the total electron charge density $\rho(r)$ as

$$E[\rho, \{R_n\}] = T[\rho] + E_{xc}[\rho] + E_C[\rho] + E_{ext}[\rho, \{R_n\}] + E_{ii}(\{R_n\}) \tag{1}$$
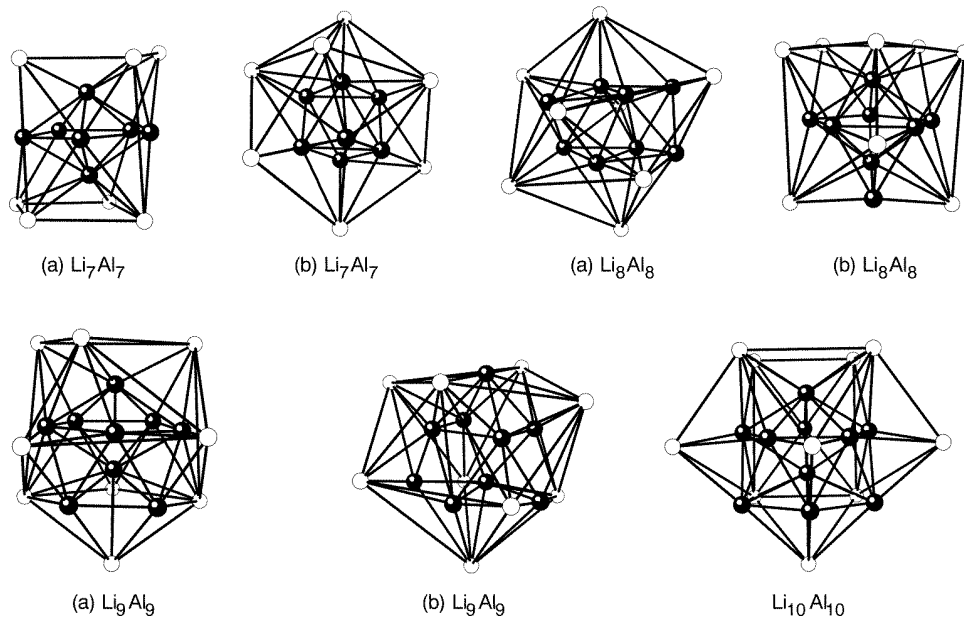
Figure 4. The ground-state (a) and low-lying (b) geometries of the Li$_7$Al$_7$, Li$_8$Al$_8$, Li$_9$Al$_9$, and Li$_{10}$Al$_{10}$ clusters.
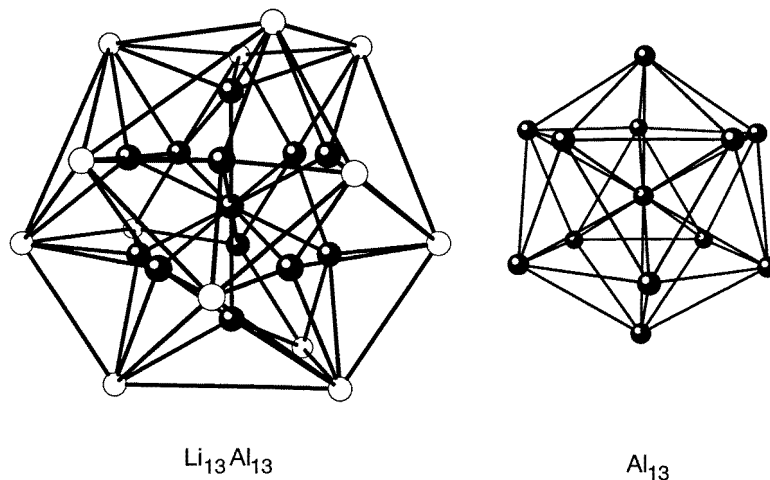

Figure 5. The ground-state geometry of Li$_{13}$Al$_{13}$, and the inner icosahedron of Al atoms.

where E_{xc} is the exchange–correlation energy, E_C is the electron–electron Coulomb interaction energy, E_{ext} is the electron–ion interaction energy, and E_{ii} is the ion–ion interaction energy. The first term—the kinetic energy functional $T[\rho]$—is approximated in the present work as
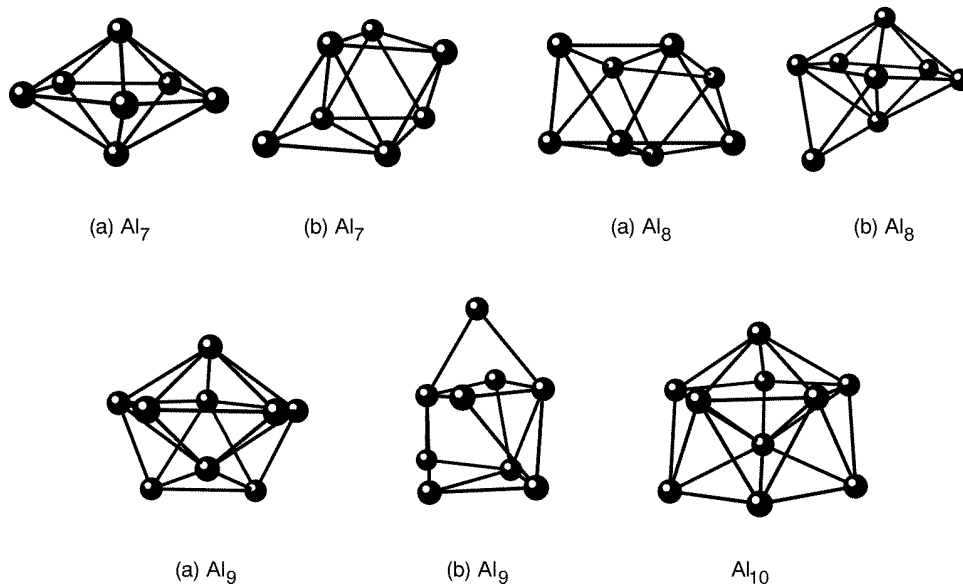
$$T[\rho] = F(N_e)T_{TF}[\rho] + T_W[\rho] \tag{2}$$

(a) Al$_7$ (b) Al$_7$ (a) Al$_8$ (b) Al$_8$

(a) Al$_9$ (b) Al$_9$ Al$_{10}$

Figure 6. The geometries of the clusters of Al atoms within the ground-state configurations of the Li$_n$Al$_n$ ($n = 7$–10) clusters.

where T_{TF} is the Thomas–Fermi term, T_{W} is the gradient correction given by Weizsacker and the factor $F(N_e)$ is

$$F(N_e) = \left(1 - \frac{2}{N_e}\right)\left(1 - \frac{A_1}{N_e^{1/3}} + \frac{A_2}{N_e^{2/3}}\right) \tag{3}$$

with optimized parameter values $A_1 = 1.314$ and $A_2 = 0.0021$ [9]. This kinetic energy functional is known to describe the response properties of the electron gas well, and has yielded very good polarizabilities for various atomic systems [10]. It also provides an excellent representation of the kinetic energy of atoms [9, 11]

The total electronic energy for a fixed geometry of atoms is minimized using the conjugate-gradient technique, and the geometry minimization has been performed using the Car–Parrinello simulated annealing strategy [12]. For the details of the formalism the reader is referred to [7]. All of the calculations were performed using only the local parts [13] of the Bachelet, Hamann and Schlüter pseudopotentials [14] for both Al and Li atoms, and the exchange–correlation potential of Ceperley and Alder as interpolated by Perdew and Zunger [15]. A periodically repeated unit cell of length 35 au with a 64 × 64 × 64 mesh and a time-step $\Delta t \sim 20$ au was used. We have chosen to use the plane-wave expansion over the entire fast-Fourier-transform mesh without any truncation, yielding the energy cut-off of 95 Ryd. During the dynamical simulated annealing, the clusters were heated to 600–850 K and then cooled very slowly to get the ground-state and low-lying energy configurations. The geometries of these clusters have been confirmed by starting with different initial configurations and also by interchanging the positions of the Li and Al atoms in a cluster and then performing a simulated annealing for 10 000–20 000 time-steps. In all of the cases the stabilities of the final ground-state configurations have been tested by reheating the clusters, allowing them to span the configuration space for a few thousand

iterations, and then slowly cooling them to obtain the low-energy configurations.

Table 1. The minimum Li–Li, Li–Al and Al–Al bond lengths (in au) of Li$_n$Al$_n$ ($n = 1$–10 and 13), as well as the eccentricity parameter η, and the symmetries of all of the clusters.

System	Li–Li	Li–Al	Al–Al	η	Symmetry
LiAl	5.51	4.77	4.14	0.99	C$_{\infty v}$
Li$_2$Al$_2$	6.71	5.05	4.17	0.60	C$_{2v}$
Li$_3$Al$_3$	7.36	5.15	4.35	0.48	C$_{2v}$
Li$_4$Al$_4$	9.08	5.31	4.50	0.43	D$_{3h}$
Li$_5$Al$_5$	6.03	5.22	4.53	0.48	C$_{2v}$
Li$_6$Al$_6$	7.55	5.37	4.60	0.40	—
Li$_7$Al$_7$	6.35	5.30	4.59	0.47	C$_{1h}$
Li$_8$Al$_8$	5.87	5.24	4.51	0.18	C$_{2v}$
Li$_9$Al$_9$	6.51	5.32	4.63	0.22	C$_{2v}$
Li$_{10}$Al$_{10}$	6.56	5.31	4.60	0.07	C$_{2v}$
Li$_{13}$Al$_{13}$	6.53	5.38	4.70	0.19	—

3. Results and discussion

3.1. Geometries

We begin the discussion by presenting the ground-state geometries of all of the clusters.

Table 1 summarizes our results for all of the clusters studied, where we have given the symmetry of each cluster, the minimum Li–Li, Li–Al and Al–Al bond lengths in au, and the eccentricity parameter η defined as $\eta = 1 - I_{\text{min}}/I_{\text{av}}$, where I_{min} is the minimum value of the moment of inertia and I_{av} the average value of the moment of inertia. η describes the deviation from an isotropic distribution around the centre. If η is small, it indicates that the cluster is nearly spherical. It can be seen that in general η decreases as the number of atoms in the cluster increases, indicating a passage towards spherical symmetry, with the Li$_{10}$Al$_{10}$ ground-state cluster being almost spherically symmetric. It is remarkable that the Li–Al and Al–Al bond lengths are more or less constant, with their ratio remaining around 0.83. These bond lengths and the ratio can be compared with the respective solid-state values for the B32 structure [2], namely, Li–Al bond length: 5.92 Å; Al–Al bond length: 5.13 Å; and ratio: ∼0.86.

In figures 1–6 the Li atoms are represented by white spheres, and the Al atoms by black spheres. A feature that is immediately noticeable for all of the geometries is the tendency of the Al atoms to form in each case an inner cluster, not necessarily at the centre, over which Li atoms get bonded. We will discuss this in detail in the following subsections, which are then followed by a discussion on stability based on the energetics, and subsequently we present the general trends seen across the entire series.

3.1.1. Li$_2$Al$_2$, Li$_3$Al$_3$, Li$_4$Al$_4$, Li$_5$Al$_5$. The ground-state geometries of these clusters are shown in figure 1. The Li$_2$Al$_2$, Li$_3$Al$_3$ and Li$_5$Al$_5$ clusters possess C$_{2v}$ symmetry whereas Li$_4$Al$_4$ has D$_{3h}$ symmetry. It is interesting to note that the Li$_2$Al$_2$ cluster is already three dimensional, unlike the clusters of Li$_4$ and Al$_4$ which are planar in their ground states. The geometries of clustered Al atoms are shown in figure 2. It can be noted that the four- and five-atom Al cores form a tetrahedron and a triangular antiprism respectively—to be

compared to their pure-state geometries which are a rhombus and a C_s structure. The Li atoms try to cap the triangular faces, as is very clearly seen in Li_4Al_4; this also happens to be one of the stable clusters, indicating that the symmetric clusters Li_2Al_3 and Li_6Al_5 (also shown in figure 1) would have enhanced stability. Indeed our simulated annealing runs performed on these clusters confirm this.

3.1.2. Li_6Al_6, Li_7Al_6, Li_8Al_6. The ground-state geometries of these clusters are shown in figure 3. In each of these the inner Al cluster forms a octahedron and the Li atoms cap the faces. This Al octahedron is the same as the one seen in the free Al_6 cluster, except for the Jahn–Teller distortion. As the number of Li atoms increases from 6 to 8, leading to the complete coverage of the Al faces of the octahedra, the stability of the clusters increases; and for Li_8Al_6 we obtain a remarkable ground-state geometry—namely FCC, with Li at the vertices and Al at the face centres.

3.1.3. Li_7Al_7, Li_8Al_8, Li_9Al_9, $Li_{10}Al_{10}$, $Li_{13}Al_{13}$. Figure 4 shows the ground-state and low-lying geometries of Li_7Al_7, Li_8Al_8, Li_9Al_9 and $Li_{10}Al_{10}$, and figure 5 shows the ground-state geometry of $Li_{13}Al_{13}$. The geometries labelled (a) are those of the ground states, whereas those labelled (b) are those of the low-lying states. All of these clusters in their ground states have C_{2v} symmetry. Again the Al atoms cluster, and their geometries are separately shown in figure 6. An interesting observation that can be made is that of the switching over in inner Al cluster geometries in going from Li_7Al_7 to Li_8Al_8 to Li_9Al_9. In the ground state of Li_7Al_7 the Al cluster is a bicapped pentagon, in Li_8Al_8 the Al cluster has distorted T_d symmetry, and in Li_9Al_9 the Al atoms form a bicapped pentagon with two faces capped, which appears to be an incomplete icosahedron. But the low-lying geometries of these clusters are reversed in the sense that they are C_{1h}, an incomplete icosahedron, and a capped T_d structure respectively. The energy difference between the ground-state and low-lying geometries for Li_7Al_7 is 0.67 eV, for Li_8Al_8 is 0.47 eV, and for Li_9Al_9 is 0.15 eV. This indicates that the presence of Li atoms drives the inner Al cluster towards an icosahedron which is completed in $Li_{13}Al_{13}$, shown in figure 5 along with the inner icosahedron of Al atoms. It may be mentioned that the Al_8 cluster is similar to the free cluster, although distorted, while Al_7, Al_9 and Al_{10} have symmetries different from those of the free clusters with the same numbers of atoms. All of these clusters show a lower η-value, of the order of 0.2, indicating evolution towards spherical geometries. It is of some interest to examine the evolution of η during the simulated annealing run. Figure 7(a) shows η as a function of the simulation time for a typical heating–cooling run; also shown is the total energy (figure 7(b)) for the case of $Li_{10}Al_{10}$. The left-hand panels show the variations up to 1200 iterations and are on a different scale to the rest of the iterations shown in the right-hand panels. Here the starting configuration has an η-value of 0.18. Starting with this non-spherical configuration, the η-value shows a sharp initial drop which correlates with the steep drop in total energy, and then starts oscillating from 0.05 to 0.14 in the first 3000 iterations, indicating that the system is spanning a wide range in the configuration space. The fluctuations in η correlate well with the energy barrier crossing, and the latter fluctuations are indicative of the oscillations around the approximate ground-state geometry having an η-value of around 0.06.
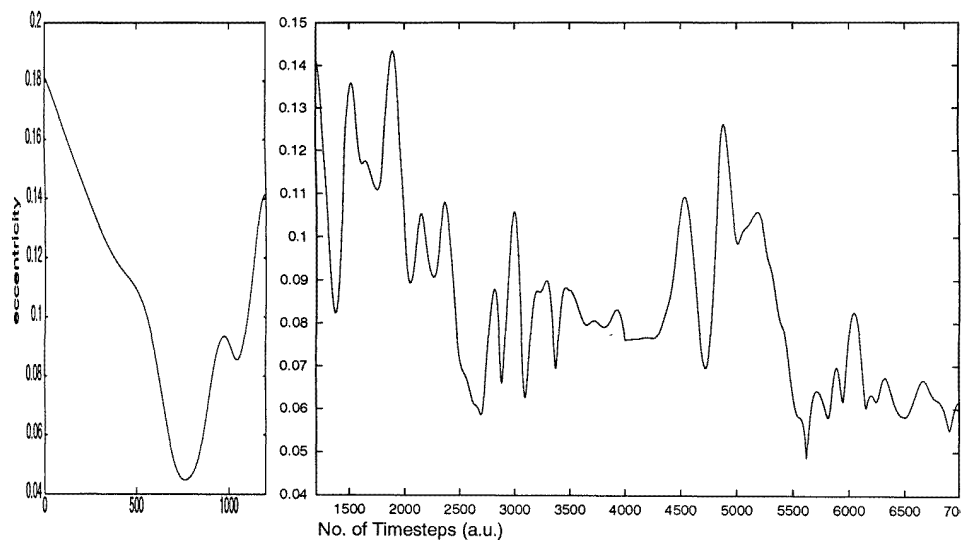
(a)
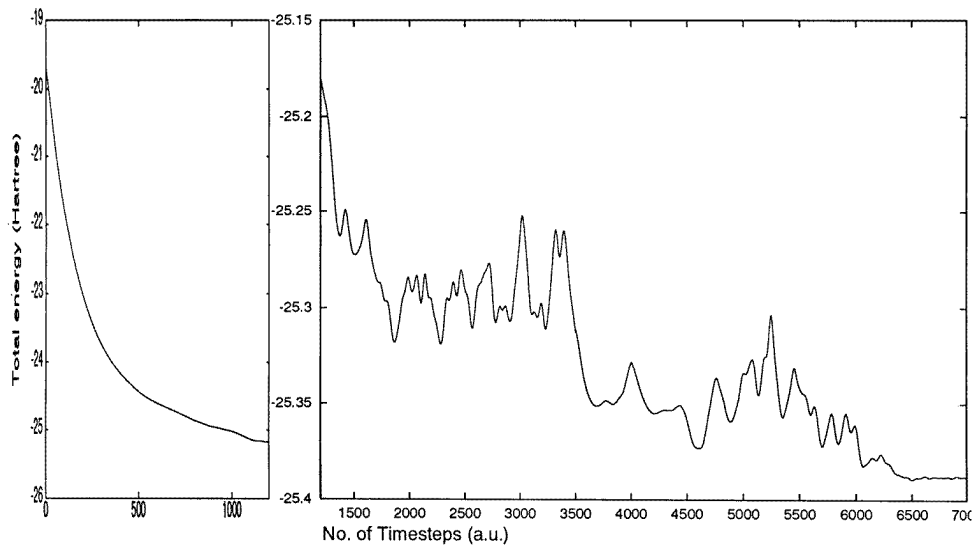
(b)

Figure 7. (a) The evolution of the eccentricity parameter η as a function of time in au. The changes in configurations, and the oscillations in configuration space can be seen. (b) The total energy in au as a function of time in au. The fluctuations in the total energy correlate with the fluctuations in η.
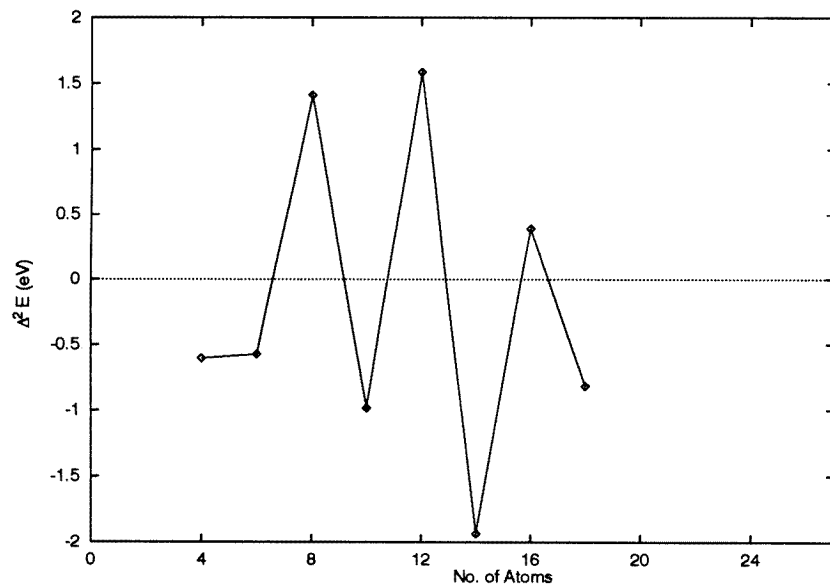
3.2. Energetics

The stabilities of the Li$_n$Al$_n$ ($n = 1$–10) clusters are now discussed on the basis of their energetics. Towards this end we define the binding energy per atom as

$$E_b[\text{Li}_n\text{Al}_m] = (-E[\text{Li}_n\text{Al}_m] + nE[\text{Li}] + mE[\text{Al}])/(n+m)$$
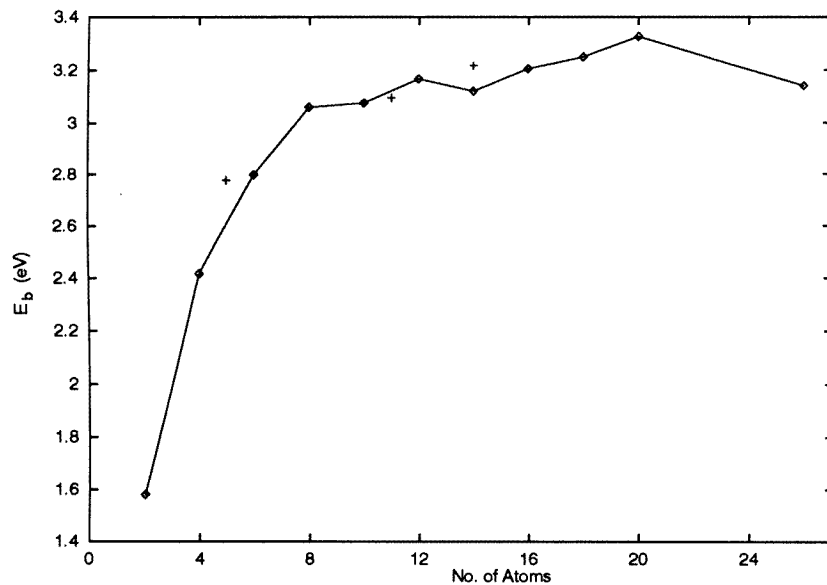
(a)

(b)

Figure 8. (a) The binding energy (in eV) for the Li_nAl_n ($n = 1$–10 and 13) clusters as a function of the total number of atoms in the cluster. (b) The second difference in energy (in eV) as a function of the total number of atoms in the Li_nAl_n ($n = 1$–10) clusters. The maxima pertain to the most stable clusters and the minima to the least stable ones. (c) The dissociation energy (in eV) as a function of the total number of atoms in the Li_nAl_n ($n = 1$–10) clusters. The minima indicate the more stable clusters and the maxima indicate the less stable ones.
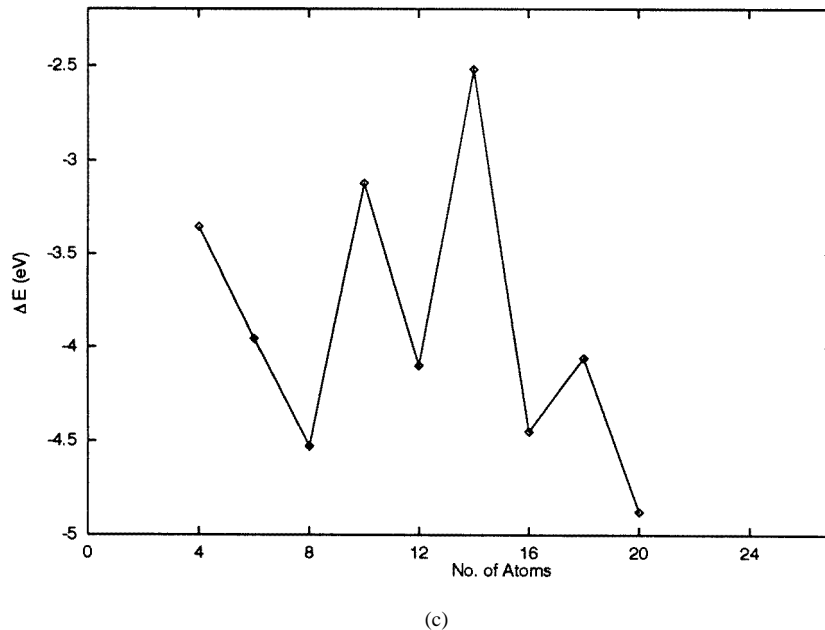
(c)

Figure 8. (Continued)

and the second difference in energy as

$$\Delta^2 E[\mathrm{Li}_n \mathrm{Al}_m] = -2E[\mathrm{Li}_n \mathrm{Al}_m] + E[\mathrm{Li}_{n+1} \mathrm{Al}_m] + E[\mathrm{Li}_{n-1} \mathrm{Al}_m]$$

and finally the dissociation energy as

$$\Delta E[\mathrm{Li}_n \mathrm{Al}_n] = E[\mathrm{Li}_n \mathrm{Al}_n] - (E[\mathrm{Li}_{n-1} \mathrm{Al}_{n-1}] + E[\mathrm{LiAl}])$$

for equiatomic clusters. These energies are shown in figure 8(a), figure 8(b) and figure 8(c) respectively. It can be seen from figure 8(a) that initially there is a sharp rise in the binding energy, and then it tapers off with the average value being at 3.2 eV. This compares well with the solid-state value of 3.42 eV [2]. The extra points in the plot are for the completely Li-covered Li$_2$Al$_3$, Li$_6$Al$_5$ and Li$_8$Al$_6$ clusters. The second differences in energies shown in figure 8(b) and the dissociation energies in figure 8(c) correlate very well, in that the most stable clusters are seen to be those with 8 and 12 atoms in total. These clusters have the *highest* second difference in energy and the *lowest* dissociation energy. All of these clusters show maximum coverage of Al faces by the Li atoms.

3.3. General trends

We end this discussion by noting the common features seen in this series of clusters. The most noticeable feature of our results is the clustering of Al atoms irrespective of the size and the relative Li/Al content of the cluster. This tendency has been confirmed by repeating the simulated annealing run, with the initial configuration having all of the Al atoms on the periphery of the cluster. It is also seen that the stable geometry of the clusters is dictated by the geometry of this Al cluster. It may be noted that the structure of the inner Al cluster is the same for the different clusters in their ground state having the same number of Al atoms, e.g Li$_6$Al$_6$ and Li$_8$Al$_6$, Li$_4$Al$_4$ and Li$_7$Al$_4$ [6]. Evidently, wherever possible the Li

atoms arrange in such a way as to maximize the Li–Al bonds with dominant tetrahedral coordination. This can be understood on the basis of the fact that the Al–Al bond is somewhat stronger than the Li–Al bond, and the cluster will stabilize itself by maximizing Li–Al bonds together with Al–Al bonds. Clearly, in a finite-size small cluster having a large surface area this can be easily achieved by placing the Li atom on the surface wherever possible. Thus the stability of the clusters is dictated by the ability of Li atoms to cap the faces of the Al surfaces. Therefore, if all of the faces of the Al cluster are capped, the structure should become more stable. This is indeed borne out by our calculations.

4. Conclusions

In the present work, we have reported our results on the geometries and stabilities of Li_nAl_n ($n = 1$–10 and 13) clusters obtained using density-based *ab initio* molecular dynamics. Our systematic investigation of these clusters indicates that there is a clustering tendency of Al atoms. The stable clusters are formed by the complete capping of all of the Al faces of these inner Al clusters by Li atoms. The Li atoms wherever possible prefer a tetrahedral coordination with the Al atoms, leading to remarkable structures like the FCC one, as in the case of Li_8Al_6. No evidence for units akin to any solid-state structures like B32 is seen in these clusters, indicating that clustering dominates over ordering tendencies. However, since in the solid phase the B32 structure is the stable ground-state structure, it is reasonable to expect that, as the cluster grows, the crossover between clustering and ordering must take place at least in the inner part of the cluster. The present clusters studied are too small to demonstrate this, and such an investigation should constitute an interesting calculation.

References

[1] Jena P, Khanna S N and Rao B K (ed) 1992 *Physics and Chemistry of Finite Systems: From Clusters to Crystals* vols 1, 2 (Dordrecht: Kluwer Academic)
[2] Arya A, Das G P, Salunke H G and Banerjee S 1994 *J. Phys.: Condens. Matter* **6** 3389
[3] Banerjee S, Das G P and Arya A 1997 *Acta Mater.* **45** 601
[4] Nehete D, Shah V and Kanhere D G 1996 *Phys. Rev.* B **53** 2126
[5] Cheng H P, Barnett R N and Landman U 1993 *Phys. Rev.* B **48** 1820
[6] Shah V and Kanhere D G 1997 *J. Phys.: Condens. Matter* **8** L253
[7] Shah V, Nehete D and Kanhere D G 1994 *J. Phys.: Condens. Matter* **6** 10 773
[8] Pearson M, Smargiassi E and Madden P A 1993 *J. Phys.: Condens. Matter* **5** 3221
    Smargiassi E and Madden P A 1995 *Phys. Rev.* B **51** 117
    Smargiassi E and Madden P A 1995 *Phys. Rev.* B **51** 129
    Smargiassi E and Madden P A 1994 *Phys. Rev.* B **49** 5220
[9] Ghosh S K and Balbas L C 1985 *J. Chem. Phys.* **83** 5778

[10] Harbola M K 1993 *Phys. Rev.* A **48** 2696
  Harbola M K 1994 *Int. J. Quantum Chem.* **51** 201
[11] Gazquez J L and Robles J 1982 *J. Chem. Phys.* **76** 1467
[12] Car R and Parrinello M 1985 *Phys. Rev. Lett.* **55** 685
[13] The local part of the pseudopotential in the present scheme consists of the potential of the core V_{core}^{ion}, which is the long-range Coulomb part (l-independent), and a short-range l-dependent pseudopotential part ΔV_l^{ion}, in which only the $l = 0$ component is used.
[14] Bachelet G B, Hamann D R and Schlüter M 1982 *Phys. Rev.* B **26** 4199
[15] Perdew J P and Zunger A 1981 *Phys. Rev.* B **23** 5048